Journal of Alloys and Compounds 607 (2014) 104–109

Contents lists available at ScienceDirect

Journal of Alloys and Compounds

journal homepage: www.elsevier.com/locate/jalcom

The phase transitions in $CsFe(MoO_4)_2$ triangular lattice antiferromagnet, neutron diffraction and high pressure studies

Anna Gągor [a,*], Paweł Zajdel [b], Daniel Többens [c]

[a] Institute of Low Temperature and Structure Research Polish Academy of Science, Okólna 2, 50-422 Wrocław, Poland
[b] University of Silesia, Institute of Physics, Katowice, Poland
[c] Helmholtz-Zentrum Berlin für Materialien und Energie GmbH, Germany

ARTICLE INFO

Article history:
Received 9 January 2014
Received in revised form 5 March 2014
Accepted 7 April 2014
Available online 18 April 2014

Keywords:
Magnetically ordered materials
Phase transitions
Neutron diffraction
Crystal structure
High pressure

ABSTRACT

We report on the phase transitions in the triangular lattice antiferromagnet $CsFe(MoO_4)_2$ at low temperatures and high pressure using powder neutron and X-ray diffraction, specific heat, magnetic susceptibility and in situ high pressure Raman measurements. $CsFe(MoO_4)_2$ undergoes a structural phase transition induced by the rotation of $(MoO_4)^{2-}$ tetrahedra at $T_c = 220$ K. The transformation is associated with a symmetry decrease from $P\text{-}3m$ to $P\text{-}3$. Below 4.5 K the antiferromagnetic long range order appears that is related to the nuclear unit cell by the modulation vector $\boldsymbol{q} = (1/3\ 1/3\ 0.5)$. The system adopts '120°' spiral spin structure that has been found in several triangular lattice multiferroics. Under pressure $CsFe(MoO_4)_2$ undergoes a reconstructive phase transition to a much larger superstructure which preserves the super-exchange interactions at low temperatures and allows an additional magnetic long-range order at $T \sim 20$ K.

1. Introduction

The electric-field control of spins and magnetic-field control of electric dipoles, beside important promising applications, opens new perspectives in the fundamental research of multiferroic materials due to rich and fascinating physics. The class of type II multiferroics, in which a specific magnetic order induces a ferroelectric phase transition, is of special interest. These so called spin-driven magneto-electrics are particularly curious because of the high magneto-electric coupling that allows controlling a ferroelectric polarization by an external magnetic field and *vice versa*. The ferroelectric polarization exists only in a magnetically ordered state and, appears as a consequence of a spiral magnetic order in most of the recently discovered type II multiferroics. Its microscopic origin may be explained by the spin-current model or the reverse Dzyaloshinskii–Moriya effect [1]. In another class of type II multiferroics ferroelectricity appears along with the collinear magnetic structure and may be explained by a symmetry-based phenomenological theory [2].

The spiral spin structures are mostly observed in magnetically frustrated systems, where the paramagnetic phase extends down to very low temperatures and the magnetic order sets as a consequence of competing magnetic interactions. A low temperature of the multiferroic phase transition is the factor that limits possible applications of these strongly coupled materials. The chemical substitutions may increase or lower the critical temperatures and change the range of the existence of subsequent phases. This applies to the magnetic as well as non-magnetic impurities. A good example is a spin-driven multiferroic $MnWO_4$ [3], in which the critical temperatures rise after Mn^{2+} substitution for Co^{2+}, whereas other magnetic ions (like Fe^{2+}, Ni^{2+}) may suppress the ferroelectric phase [4,5]. On the other hand, the largest increase of the T_N is observed when the nonmagnetic W^{6+} is substituted for nonmagnetic Mo^{6+} indication that tiny changes in the local crystal structure may effectively contribute to the magneto-electric coupling [6].

The most typical examples of frustrated spin systems are triangular lattice antiferromagnets which accommodate complex spin structures due to the geometric frustration. The appearance of polarization at T_N has recently been reported for $RbFe(MoO_4)_2$ triangular lattice antiferromagnet which adopts '120°' spin structure in the ground state with the spin spiral confined in the plane as well as in Cu and $AgCrO_2$ delafossities, which are easy-axis triangular magnets also adopting '120°' spin structure [7,8].

The $RbFe(MoO_4)_2$ belongs to the family of magnetic solids with $AM(XO_4)_2$ composition, where A is an alkali metal, M: magnetic ion (Cr^{3+}, Fe^{3+} or Mn^{3+}); X: Mo, W, S, Se [9]. All the compounds exhibit a rich polymorphism of their layered, trigonal crystal structures.

* Corresponding author. Tel.: +48 71 3954145.
E-mail address: a.gagor@int.pan.wroc.pl (A. Gągor).

http://dx.doi.org/10.1016/j.jallcom.2014.04.049
0925-8388/

The $RbFe(MoO_4)_2$ is isotypic to $KAl(MoO_4)_2$ which crystallizes in *P*-3*m*1 symmetry [10]. The most important feature of this structure is its quasi two-dimensional character. Magnetic ions are located on the triangular lattices and stack along *c* direction. They are separated by MoO_4^{2-} tetrahedra and alkaline metal ions, see Fig. 1. The quasi 2-D triangular arrangement of the Fe^{3+} ions leads to the geometric frustration of the spin system. As a result the incommensurately modulated antiferromagnetic order with the magnetic propagation vector $\boldsymbol{q} = (1/3\,1/3\,0.448)$ sets at a very low temperature $T_N \sim 3.7$ K together with the ferroelectric phase. The multiferroic phase transition is preceded by a structural distortion at $T_c = 190$ K associated with the symmetry decrease from *P*-3*m*1 to *P*-3 [11].

Despite the fact that extensive scientific studies have been devoted to $RbFe(MoO_4)_2$ there are not many reports on its cesium analogue, $CsFe(MoO_4)_2$. This is probably due to the difficulties with the single crystal growth of these materials, although single-crystals suitable for X-ray diffraction have been obtained and structurally characterized by Bazarov et al. [12]. At room temperature $CsFe(MoO_4)_2$ is isostructural with $RbFe(MoO_4)_2$ and $KAl(MoO_4)_2$ and has similar quasi-2D crystal structure. It crystalizes in a centrosymmetric *P*-3*m*1 rhombohedral space group with a unit cell: $a = b = 5.6051(2)$ Å, $c = 8.0118(4)$ Å and $\gamma = 120°$. Lattice parameters correspond to the inter- and intra- Fe^{3+}–Fe^{3+} distances for *a*, *b* and *c*, respectively. The inter-to-intra layer distance ratio *c*/*a* equals 1.43 and is higher than the one observed in $RbFe(MoO_4)_2$, where $c/a = 1.31$, indicating better separation of magnetic layers.

The chemical substitutions may change the phase diagram in multiferroic crystals thus promoting or suppressing desired properties. Here, we report experimental evidence that $CsFe(MoO_4)_2$ may be a type-II multiferroic with transition temperature $T_N \sim 4.7$ K. The phase situation concerning the crystal as well as the magnetic structure changes and its high pressure behavior are discussed on the basis of the powder neutron and X-ray diffraction and Raman scattering. Also the preliminary results for the high pressure phase, obtained after the reconstructive phase transition, are reported. They differ considerably from recently published pressure-induced changes in $RbFe(MoO_4)_2$ [13].

2. Experimental

The red, fine powders of $CsFe(MoO_4)_2$ were obtained by the flux method from Cs_2CO_3, Fe_2O_3 and MoO_3 starting materials. The mixture was placed in a platinum crucible and heated in air in a furnace up to 800 °C for 20 h, cooled at 2 °C/h to 500 °C and subsequently at 5 °C/h to room temperature. During the synthesis there were oxidizing conditions giving the powder the brownish-red color.

The specific heat measurements were performed on the sintered specimens using a Quantum Design PPMS platform. The heat capacity measurements were carried out over the temperature interval 2–350 K, employing a thermal relaxation technique [14]. The magnetization was measured using a Quantum Design MPMS-5 SQUID magnetometer.

The Raman spectra were measured using Renishaw InVia Raman spectrometer equipped with confocal DM 2500 Leica optical microscope, a thermoelectrically cooled Ren Cam CCD as a detector and a diode laser operating at 830 nm. The spectral resolution was 2 cm^{-1}. The high pressure for Raman experiment was maintained in Merrill-Bassett diamond anvil cell. The pressure was controlled using single crystal X-ray diffraction of CaF_2.

The neutron powder diffraction was measured on the Fine Resolution Powder Diffractometer E9 at Helmholtz Zentrum Berlin. The detector consisting of eight individual 2D detectors with 300 × 300 mm active area and a radial collimator to reduce background noise was used; $\lambda = 1.7982(1)$ Å from Ge(5 1 1), angle resolution was 0.33°.

3. Results and discussion

3.1. The thermal properties of $CsFe(MoO_4)_2$

Fig. 2 shows the temperature dependences of the inverse molar susceptibility $\chi^{-1} = (M/H)^{-1}$ for the 'as prepared' $CsFe(MoO_4)_2$ and pressed at 2 GPa, measured in an external magnetic field of $H = 10$ kOe on cooling for temperatures $1.9\ K \leqslant T \leqslant 400$ K. For the 'as prepared' sample the magnetic susceptibilities exhibit an extended range of the Curie–Weiss (CW) behavior down to 8 K. Below that, a clear antiferromagnetic anomaly appears at $T_N = 4.5$ K. The frustration parameter defined as the ratio of the absolute value of the CW temperature Θ_p to the transition temperature T_N, *i.e.* $f = |\Theta_p|/T_N$ is close to 6 indicating a moderate frustration of the spin system (for strongly frustrated phases $f > 10$). In the sample that was initially compressed to ~2 GPa, then recovered to ambient pressure an additional long range magnetic order appears at $T \sim 20$ K that is followed by the onset of antiferromagnetic phase with a lower Neel temperature, $T_N \sim 3.9$ K. Fig. 2(b) shows the total heat capacity of the sintered sample measured in zero field. A reversible phase transition is observed at $T_c = 220$ K. The absence of a temperature hysteresis implies a continuous character of this transformation. The magnetic phase transition gives the contribution to the specific heat at $T_N = 3.5$ K.

3.2. The crystal structure at low temperatures from the neutron diffraction

The neutron diffraction patterns of $CsFe(MoO_4)_2$ measured at 7 and 2 K together with the Rietveld refinement results are presented in Figs. 3 and 4. At 7 K a satisfactory fit to the experimental data is possible using lower symmetry of the crystal structure than reported for the room temperature phase [11]. Initial refinement in the P-3m1 symmetry at 7 K with O(2) oxygen atoms located on .m. planes did not lead to convergence, giving high discrepancy factors (R_B: 26, R_F: 18 and $R_P = 37$) and pronounced residua on difference diagrams.

The $CsFe(MoO_4)_2$ undergoes a structural distortion at low temperatures and its symmetry is reduced from *P*-3*m*1 to *P*-3 at 220 K.

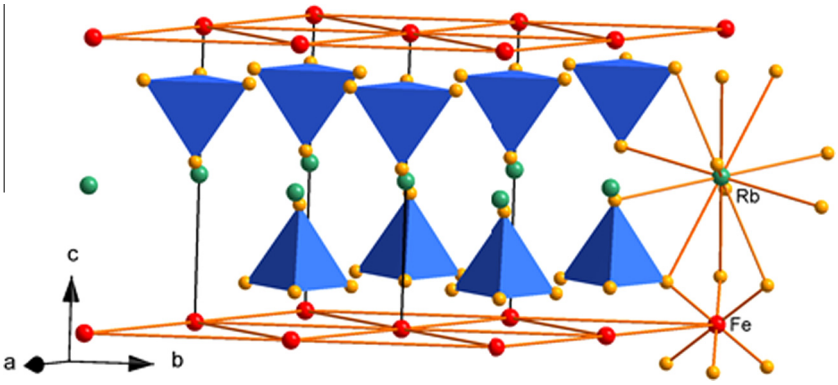

Fig. 1. The characteristic features of a quasi-2D crystal structure of $RbFe(MoO_4)_2$ and $KAl(MoO_4)_2$ compounds.

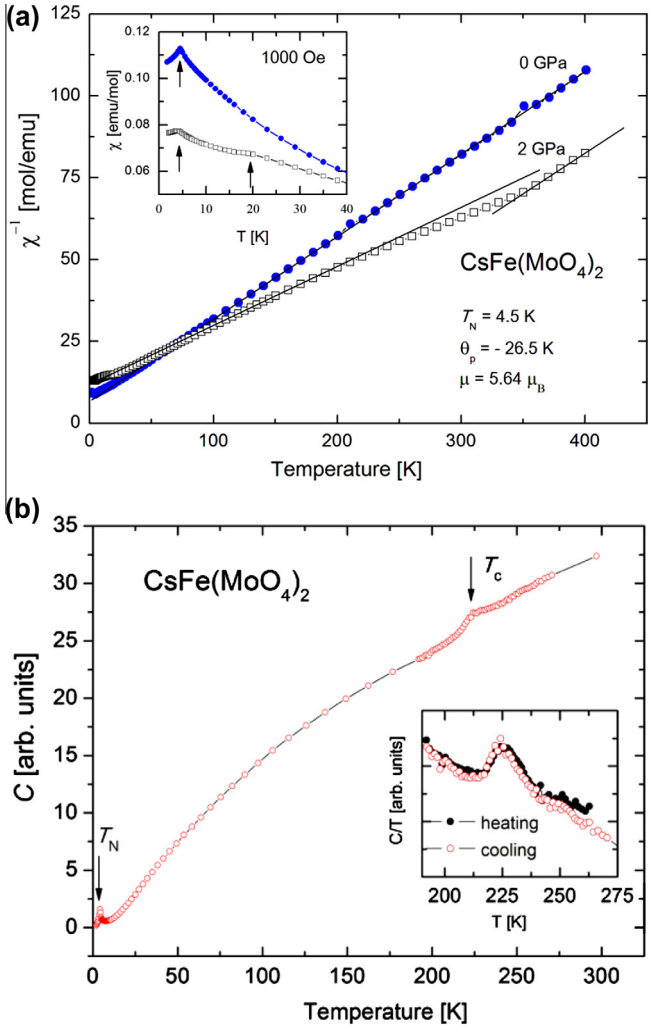

Fig. 2. (a) An inverse magnetic susceptibility for $CsFe(MoO_4)_2$ as prepared and pressed under 2 GPa and (b) the heat capacity for the pristine sample, the inset details the structural phase transition at $T_c = 220$ K.

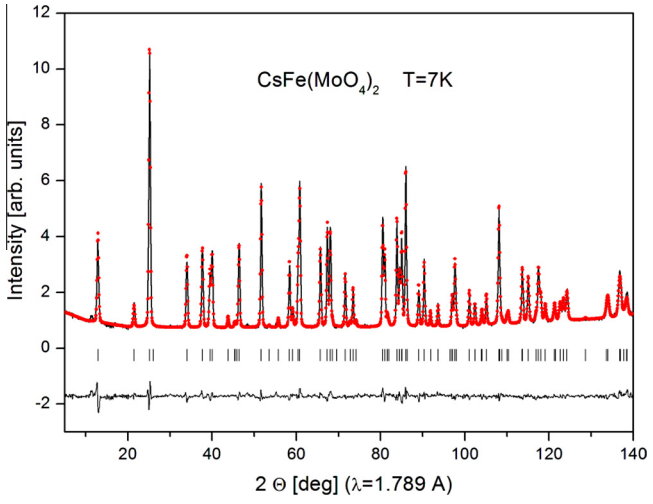

Fig. 3. The results of the Rietveld refinement for $CsFe(MoO_4)_2$ in the paramagnetic state at 7 K: experimental, calculated and difference plots, space group *P*-3, $R_{wp} = 8.57$, $R_{exp} = 5.68$ Bragg *R*-factor = 4.323, $\chi^2 = 2.27$; R_F-factor = 3.242.

A similar transition is observed in $RbFe(MoO_4)_2$ at $T_c = 190$ K. The distortion is associated with the rotation of $(MoO_4)^{2-}$ tetrahedra around the *c*-axis which removes *.m.* mirror plane. In all layers, the tetrahedra rotate in the same direction. Fig 5 illustrates the arrangement of $(MoO_4)^{2-}$ and FeO_6 polyhedra before and after the phase transition. The distortion entails also the reduction of the local symmetry of Mo^{6+} and Fe^{3+} ions from 3*m*. to 3.. and from $-3m.$ to $-3..$, respectively. The rotation angle is large and equals $\sim 14°$.

Below $T_N = 4.5$ K discrete magnetic peaks appear as a result of antiferromagnetic long range order. They may be indexed using the magnetic propagation vector $\boldsymbol{q} = (1/3\,1/3\,0.5)$ in respect to the nuclear trigonal unit cell. The crystal structure symmetry *P*-3 persists in the ordered magnetic phase. Table 1 contains the structural parameters obtained from the neutron powder diffraction at 7 and 2 K. The temperature dependence of the magnetic Bragg peak area intensity is shown in Fig. 5(b). The continuous character of the changes points to the second-order character of the phase transition. To refine the magnetic structure of $CsFe(MoO_4)_2$ the models with all spins confined in (a, b) plane were applied using formalism of irreducible representations of propagation vector group implemented in Fullprof and program SARAh [15]. Models with spins confined from the (a, b) plane were also checked. They gave, however, peaks in positions that did not much the observed neutron diffraction patterns.

In $CsFe(MoO_4)_2$ the spin arrangement may be described by two complex scalar order parameters $\sigma^{(1,2)}(q_z)$, according to which the spin distribution may be reproduced using the equations:

$$S_x(r) = \left[\sigma^{(1)}(q_z) + \sigma^{(2)}(q_z)\right] \exp(i\mathbf{qr})$$

$$S_y(r) = i\left[\sigma^{(1)}(q_z) + \sigma^{(2)}(q_z)\right] \exp(i\mathbf{qr})$$

Since these two states are degenerate in energy the magnetic structure is described by either $\sigma^{(1)} = \sigma$ and $\sigma^{(2)} = 0$ or *vice versa*, $\sigma^{(1)} = 0$ and $\sigma^{(2)} = \sigma$, depending on the sign of the chirality [2]. The spin rotation between the triangular layers is determined by q_z. The spins in the adjacent planes are rotated by an angle $2\pi q_z$, which equals 180° for $q_z = 0.5$ giving AF setting. As far as the spin arrangement in (a, b) plane is concerned, a good fit to the experimental data gives so called '120°' spin structure in which a spin on the triangular lattice rotates by 120° clock wise or counter-clockwise when it moves to the neighboring site. The results of the Rietveld refinement together with reliability factors are shown in Fig. 4(a). The spin arrangement for '120°' spin structure in $CsFe(MoO_4)_2$ in the base cell, in the (a, b) plane and in the $3 \times 3 \times 1$ superstructure is illustrated in Fig. 6(a)–(c), respectively.

The '120°' magnetic structure has been reported for multiferroic $RbFe(MoO_4)_2$ [2,7]. Kanzelman et al. introduced a symmetry based phenomenological theory to explain the presence of a magnetoelectric phase in this system. It appears that ferroelectricity is a generic property of the quasi 2D Heisenberg anti-ferromagnets on the triangular lattice that under special symmetry conditions develop '120°' spin structures. Worthy of note is that the incommensurability ($q_z \sim 0.46$) observed in $RbFe(MoO_4)_2$ is not a requirement for the magnetoelectricity. The main component that allows for the induction of polarization is associated with the symmetry of the crystal lattice. It turns out that the essential ingredient of the magnetoelectricity is the absence of a mirror plane perpendicular to the c axis (as it is in *P*-3 space group). The general rule is that ferroelectric polarization appears when a magnetic structure breaks inversion symmetry and defines a unique direction. The '120°' spin structure is chiral, thus it breaks the inversion center whereas the direction of the spiral rotation defines a unique direction. On the microscopic level the ferroelectricity appears as a consequence of Dzyaloshinskii–Moriya interaction between nearest in-plane neighbors when the unit vector connecting them neither includes a mirror plane, nor is perpendicular to the twofold

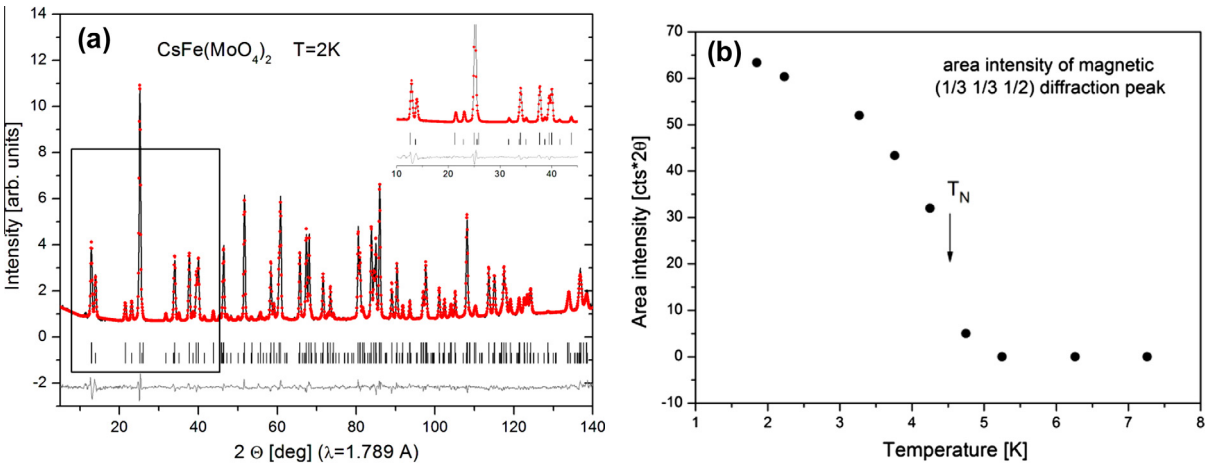

Fig. 4. (a) The results of the Rietveld refinement for $CsFe(MoO_4)_2$ at 2 K in the antiferromagnetic phase. Reliability factors for profile: R_p = 3.91, R_{wp} = 4.79, R_{exp} = 2.98, χ^2 = 2; for nuclear structure: bragg *R*-factor = 4.59, R_F = 3.54; magnetic *R*-factor = 12.9; (b) area intensity of the (1/3 1/3 0.5) magnetic peak, the line is plotted only as a guide for the eye.

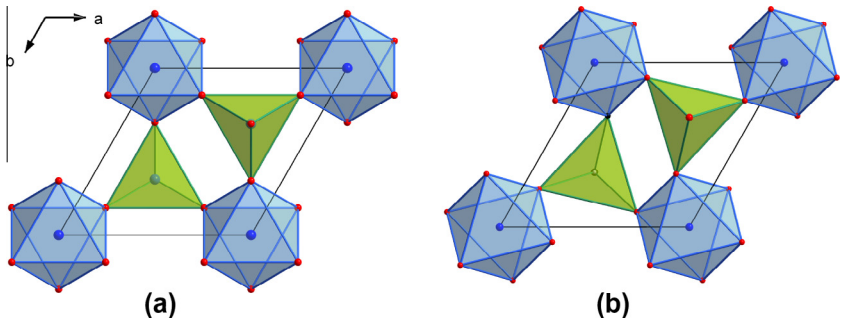

Fig. 5. The view of the crystal structure of the $CsFe(MoO_4)_2$ at room temperature (a) and 7 K (b). The structural distortion, that appears at T_c = 220 K, reflects in a rotation of $(MoO_4)^{2-}$ and FeO_6 polyhedra. The symmetry lowers from *P*-3*m*1 to *P*-3.

Table 1
The structure parameters for $CsFe(MoO_4)_2$ at 7 K in the paramagnetic phase and 2 K (the antiferromagnetic phase) obtained from the Rietveld refinement.

Atom	Site	Symm.	x	y	z
System trigonal; space group P -3 (147)					
7 K		a = 5.5652(1) Å	c = 7.9794(1) Å	V = 214.02(0) Å^3	
Cs	1b	−3..	0	0	1/2
Fe	1a	−3..	0	0	0
Mo	2d	3..	1/3	2/3	0.2124(3)
O1	2d	3..	1/3	2/3	0.4284(4)
O2	6g	1	0.2314(3)	0.3232(4)	0.1470(3)
2 K		a = 5.5646(1) Å	c = 7.9796(1) Å	V = 213.98(0) Å^3	
Cs	1b	−3..	0	0	1/2
Fe	1a	−3..	0	0	0
Mo	2d	3..	1/3	2/3	0.2127(3)
O1	2d	3..	1/3	2/3	0.4282(4)
O2	6g	1	0.2321(3)	0.3236 (3)	0.1471(3)

rotation axis [16]. The spin current model [1] is expected to produce polarization in a basal plane thus cannot explain the emergence of P_c in these systems.

Similarly to the rubidium analogue the value of the measured saturation magnetization obtained from the magnetic susceptibility measurement is lower than 5 μ_B expected for the ^6S ground state of Fe^{3+}. The value of the magnetic moment obtained from the neutron study is even lower and equals to 4.01(5) μB. It may be explained by a nonmagnetic sample contamination; however, it may also point to some discrepancies from the ideal '120°' spin structure. An alternative solution of the magnetic structure, giving the same fit to the diffraction data, produces a remarkably different spin arrangement in the (a, b) plane which consists of antiparallel spins set on a honey-comb nods and a not defined (disordered) spin configuration in the middle, see Supplementary materials S1.

3.3. The high pressure phase transition in $CsFe(MoO_4)_2$

$CsFe(MoO_4)_2$ experiences a reconstructive phase transformation during the compression. In ambient conditions the Raman spectrum of $CsFe(MoO_4)_2$ is similar to the one recorded for multiferroic $RbFe(MoO_4)_2$ [17]. Before reaching ~0.7(1) GPa a reconstructive PT takes place to a much lower symmetry. The spectrum characteristic for the new phase remains unchanged up to 3.5 GPa. There is no trace of the ambient pressure phase in the Raman spectra after the compression which evidences that the whole sample transformed to the new phase. After a decompression the new phase is stabilized at ambient conditions. A reconstructive character of the high pressure phase also has been reported for $RbFe(MoO_4)_2$ and $KFe(MoO_4)_2$ crystals [18,17]. Fig. 7 presents the pressure dependence of Raman spectra for $CsFe(MoO_4)_2$ together with the modes assignment based on Maczka's paper [17]. After the transformation the number of observed bands increases significantly and the energy gap between the stretching and bending modes drastically decreases from 413 cm^{-1} to 116 cm^{-1}. The bending and stretching modes spread over broad regions (from 306 to 483 and from 600 to 959 cm^{-1}) which denote much larger distribution of Mo–O distances compare to ambient conditions. Also the sharp and intense mode at 933 cm^{-1}, which corresponds to the vibration of oxygen

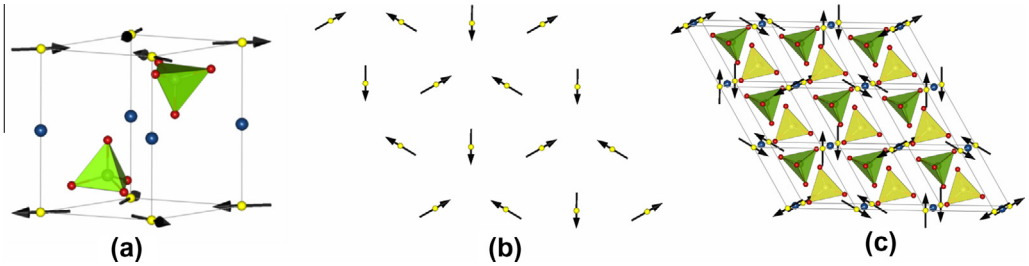

Fig. 6. (a) The spin arrangement in a basic crystallographic cell at 2 K. Fe^{3+} are shown in yellow, Cs^{+} in blue, O^{2-} in red and Mo^{6+} in green; (b) the spin distribution in an ideal '120°' spin structure on a basal plane and (c) the magnetic structure in $3 \times 3 \times 1$ supercell, the spins set AF along c axis. (For interpretation of the references to color in this figure legend, the reader is referred to the web version of this article.)

interacting with Cs^{+} ion, decreases rapidly after the transition. It indicates that also Cs–O bonds are much affected by the transition. Upon further compression the spectra remain qualitatively the same but all modes are slightly blue shifted. The changes observed in Raman spectra are in accordance with the X-ray diffraction measurement done for $CsFe(MoO_4)_2$ after the pressure recovery.

The powder diffraction diagram for the sample having been compressed up to 2 GPa and then recovered to the ambient conditions reveals much reduction of the crystal symmetry. The diffraction lines of the high pressure phase are much broader than those observed for the pristine phase significantly complicating a proper indexing. The peak broadening may be the result of a residual strain or a significant disorder of the crystal structure. A high background with a wide hallo evidences the presence of an amorphous phase. All diffraction peaks may be, however, indexed in the large monoclinic or pseudo-monoclinic super-cell with parameters $a' = 13.70(1)$, $b' = 9.75(1)$ Å, $c' = 9.80(1)$ Å and $\beta = 94.74(1)°$; related to the hexagonal cell by [20−1,120,101] transformation. Fig. 8 Presents a La Bail fit of the diffraction patterns after the compression using the monoclinic superstructure. The parameter b' is related to the distance between the atoms within the hexagonal layer and it does not change much after the compression (in ambient conditions it equals 9.708(1) Å [12]). This implies that the transformation does not affect much the intra-layer Fe–Fe distances. The parameters a' and c' are related to the mutual position of the every second hexagonal layers. The monoclinic angle β is a measure of the deformation which is possibly a cleavage shift of the layers. In this pseudo-monoclinic setting the volume after transformation is 6 times greater than before and the Z number increase from 1 to 6, which implies the maximal number of independent $(MnO_4)^{2-}$ groups being equal to 6 (for P-1 symmetry which has general positions with multiplicity equal to 2). The Raman spectra as well as X-ray powder data indicate that after the compression $CsFe(MoO_4)_2$ undergoes a reconstructive phase transition without a trace of the pristine phase. The Raman spectra of $CsFe(MoO_4)_2$ and $RbFe(MoO_4)_2$ are qualitatively the same above 1 GPa suggesting similar type of the crystal structure for both compounds at high pressure. The powder data however, are not consistent with the recent report on the high pressure structure of $RbFe(MoO_4)_2$ [13]. By measuring a two-phase system in non-hydrostatic conditions the authors show that above 1 GPa $RbFe(MoO_4)_2$ is isotypic to $RbNd(WO_4)_2$ with $C2/c$ symmetry and lattice parameters $a'_m \sim b'_m \sim 2a$ and $c'_m \sim c$ and $\beta \sim 115°$. For $CsFe(MoO_4)_2$ this type of the unit cell does not give a satisfactory indexing, alternatively a larger monoclinic cell is suggested.

Taking into account the magnetic properties of the high pressure phase our results also differ from those reported for the rubidium analog [13]. Instead of vanishing long range magnetic interactions an additional long range magnetic order appears in the high pressure phase at $T \sim 20$ K (see Fig. 2(a)) that is followed by the onset of an antiferromagnetic phase at $T_N \sim 3.9$ K. The presence of the magnetic order in the high pressure superstructure corroborates the moderate changes in the iron substructure after the compression and preservation of super-exchange interactions.

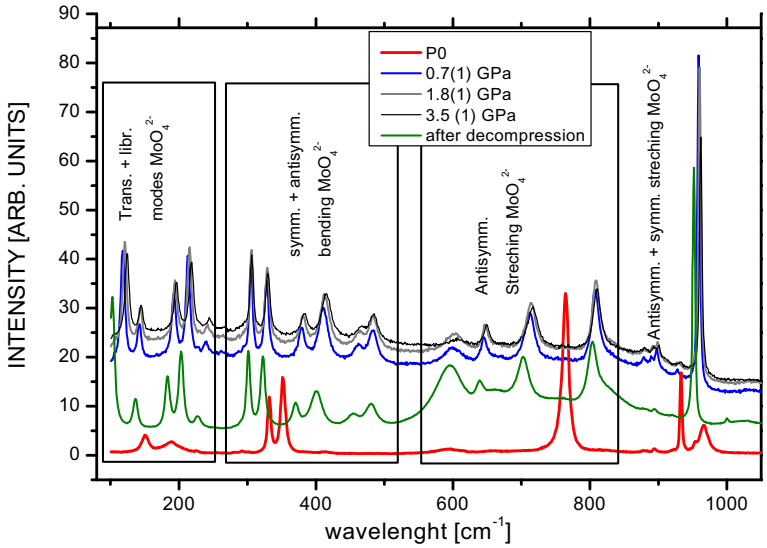

Fig. 7. The high-pressure Raman spectra for $CsFe(MoO_4)_2$.

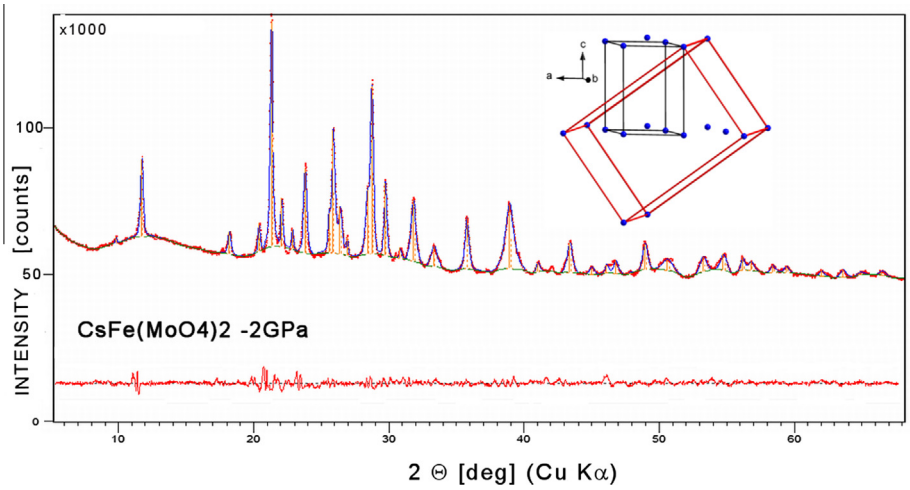

Fig. 8. The powder diffraction diagram of the sample compressed at 2 GPa and subsequently recovered to ambient conditions. All peaks may be indexed in a monoclinic cell (with lattice parameters a = 13.70(1) Å, b = 9.75(1) Å, c = 9.80(1) Å, β = 94.74(1)°. The difference plot (at the bottom) shows the results of a La Bail fit. The inset presents a relation between a trigonal cell (black) and a possible superstructure (red). (For interpretation of the references to color in this figure legend, the reader is referred to the web version of this article.)

4. Conclusions

Based on the powder neutron diffraction data, the specific heat and the magnetic susceptibility measurements we have shown that $CsFe(MoO_4)_2$ crystals develop long range magnetic order (so called '120°' spin structure) below T = 4.5 K. Combining the results with the reports for $RbFe(MoO_4)_2$ and the triangular lattice delafossites, $CsFe(MoO_4)_2$ is expected to be multiferroic type II material with a spontaneous polarization induced by the spin configuration. The crystal as well as the magnetic structure at low temperatures are similar to those found for multiferroic $RbFe(MoO_4)_2$. The chemical substitution with isovalent metal ion changes the magnetic transition temperature in iron molybdates from 3.7 to 4.5 K (for rubidium and cesium analogs, respectively). The $CsFe(MoO_4)_2$ undergoes a structural phase transition induced by the rotation of $(MoO_4)^{2-}$ tetrahedra at T_c = 220 K. The transformation is associated with a symmetry decrease from P-3m to P-3. Below 4.5 K antiferromagnetic long range order appears. It is related to the nuclear unit cell by the modulation vector $\boldsymbol{q}$ = (1/3 1/3 0.5). The modulation vector, as opposed to the rubidium analogue, does not show any deviation from the commensurability.

It has been evidenced that $CsFe(MoO_4)_2$ undergoes the reconstructive phase transition between an ambient and 0.7 GPa pressure. Due to the rotation of $(MnO_4)^{2-}$ tetrahedra and FeO_6 octahedra the pressure induces large changes in the Mo–O–Fe distances and angles which manifests themselves in a varied distribution of the Raman modes. The preliminary results demonstrate that the high-pressure phase transition leads to a monoclinic or a pseudo-monoclinic superstructure which preserves the magnetic super-exchange interactions at low temperatures and allows an additional magnetic long-range order at $T \sim 20$ K.

Acknowledgements

We thank HZB for the allocation of neutron radiation beam time. The work was supported by the Polish State Committee for Scientific Research (Project Register No. NN202 260 939), the research leading to these results has also received funding from the *European Commission under the 7th Framework Programme through the 'Research Infrastructure' action of the 'Capacities' Programme*, *NMI3-II Grant Number* 283883. The authors thank also dr Daniel Gnida for specific heat and magnetic susceptibility measurements.

Appendix A. Supplementary material

Supplementary data associated with this article can be found, in the online version, at http://dx.doi.org/10.1016/j.jallcom.2014.04.049.

References

[1] H. Katsura, N. Nagaosa, A.V. Balatsky, Phys. Rev. Lett. 95 (5) (2005) 057205.
[2] M. Kenzelmann, G. Lawes, A.B. Harris, G. Gasparovic, C. Broholm, A.P. Ramirez, G.A. Jorge, M. Jaime, S. Park, Q. Huang, A.Ya. Shapiro, L.A. Demianets, Phys. Rev. Lett. 98 (26) (2007) 267205.
[3] O. Hayer, N. Hollmann, I. Klassen, S. Jodlauk, L. Bohaty, P. Becker, J.A. Mydosh, T. Lorentz, D. Khomskii, J. Phys.: Conden. Matter. 18 (2006) L471–L475.
[4] Y.S. Song, J.H. Chung, J.M.S. Park, Y.N. Choi, Phys. Rev. B B79 (2009) 224415.
[5] R.P. Chaundry, B. Lorentz, Y.Q. Wang, Y.Y. Sun, C.W. Chu, New J. Phys. 11 (2009) 033036.
[6] L. Meddar, M. Josse, M. Maglione, A. Guiet, C. La, P. Deniard, R. Decourt, Ch. Lee, Ch. Tian, S. Jobic, M.-H. Whangbo, Ch. Payen, Chem. Mater. 24 (2012) 153.
[7] T. Inami, J. Solid State Chem. 180 (7) (2007) 2075–2079.
[8] S. Seki, Y. Onose, Y. Tokura, Phys. Rev. Lett. 101 (2008) 067204.
[9] R.F. Klevtsova, Kristallografiya 15 (1970) 209.
[10] R.F. Klevtsova, P.V. Klevtsov, Kristallografiya 15 (1970) 953–959.
[11] A. Waśkowska, L. Gerward, J. Staun, J. Olsen, W. Morgenroth, M. Maczka, K. Hermanowicz, J. Phys. Conden. Matter. 22 (5) (2010) 055406.
[12] B.G. Bazarov, T.V. Namsaraeva, R.F. Klevtsova, A.G. Anshits, T.A. Vereshchagina, L.A. Glinskaya, K.N. Fedorov, Zh.G. Bazarova, Crystall. Reports 55 (4) (2010) 591–593.
[13] D.P. Kozlenko, S.E. Kichanov, E.V. Lukin, N.T. Dang, L.S. Dubrovinsky, E.A. Bykova, K.V. Kamenev, H.-P. Liermann, W. Morgenroth, A.Y. Shapiro, B.N. Savenko, Phys. Rev. B 87 (1) (2013) 014112.
[14] J.S. Hwang, K. Lin, C. Tien, Rev. Sci. Inst. 68 (1997) 94.
[15] A.S. Wills, Physica B 276 (2000) 680.
[16] J.S. White, Ch. Niedermayer, G. Gasparovic, C. Broholm, J.M.S.A. Park, Ya. Shapiro, L.A. Demianets, M. Kenzelmann, Phys. Rev. B 88 (2013) 060409(R).
[17] M. Maczka, M. Ptak, C. Luz-Lima, P.T.C. Freire, W. Paraguassu, S. Guerini, J. Hanuza, J. Solid State Chem. 184 (10) (2011) 2812–2817.
[18] M. Maczka, A. Pietraszko, G.D. Saraiva, A.G.S. Filho, W. Paraguassu, V. Lemos, C.A. Perottoni, M.R. Gallas, P.T.C. Freire, P.E. Tomaszewski, F.E.A. Melo, J.M. Filho, J. Hanuza, J. Phys. Conden. Matter. 17 (39) (2005) 6285–6300.